Nuclear Instruments and Methods in Physics Research A 837 (2016) 1–10

Contents lists available at ScienceDirect

Nuclear Instruments and Methods in Physics Research A

journal homepage: www.elsevier.com/locate/nima

The ROSPHERE γ-ray spectroscopy array

D. Bucurescu [a], I. Căta-Danil [a], G. Ciocan [a], C. Costache [a], D. Deleanu [a], R. Dima [a], D. Filipescu [a,c], N. Florea [a], D.G. Ghiţă [a], T. Glodariu [a], M. Ivaşcu [a], R. Lică [a], N. Mărginean [a], R. Mărginean [a], C. Mihai [a,*], A. Negret [a], C.R. Niţă [a], A. Olăcel [a], S. Pascu [a], T. Sava [a], L. Stroe [a], A. Şerban [a,i], R. Şuvăilă [a], S. Toma [a], N.V. Zamfir [a,c], G. Căta-Danil [b], I. Gheorghe [c], I.O. Mitu [c], G. Suliman [c], C.A. Ur [c], T. Braunroth [d], A. Dewald [d], C. Fransen [d], A.M. Bruce [e], Zs. Podolyák [f], P.H. Regan [f,g], O.J. Roberts [h]

[a] Horia Hulubei National Institute of Physics and Nuclear Engineering - IFIN-HH, R-077125 Bucharest, Romania
[b] Physics Department, University "Politehnica" of Bucharest, Bucharest, Romania
[c] Extreme Light Infrastructure Nuclear Physics - ELI-NP, Horia Hulubei National Institute of Physics and Nuclear Engineering - IFIN-HH, R-077125 Bucharest, Romania
[d] Institut für Kernphysik der Universität zu Köln, D-50937 Köln, Germany
[e] School of Computing, Engineering and Mathematics, University of Brighton, Brighton BN2 4GJ, UK
[f] Department of Physics, University of Surrey, Guildford GU2 7XH, UK
[g] National Physics Laboratory, Teddington TW11 0LW, UK
[h] School of Physics, University College Dublin, Belfield Dublin 4, Ireland
[i] Faculty of Physics, University of Bucharest, 077125 Bucharest, Romania

ARTICLE INFO

Article history:
Received 23 February 2016
Received in revised form
5 August 2016
Accepted 24 August 2016
Available online 27 August 2016

Keywords:
γ-Ray spectroscopy
Lifetime measurements

ABSTRACT

The ROmanian array for SPectroscopy in HEavy ion REactions (ROSPHERE) has been designed as a multi-detector setup dedicated to γ-ray spectroscopy studies at the Bucharest 9 MV Tandem accelerator. Consisting of up to 25 detectors (either Compton suppressed HPGe detectors or fast $LaBr_3(Ce)$ scintillator detectors) together with a state of the art plunger device, ROSPHERE is a powerful tool for lifetime measurements using the Recoil Distance Doppler Shift (RDDS) and the in-beam Fast Electronic Scintillation Timing (FEST) methods. The array's geometry, detectors, electronics and data acquisition system are described. Selected results from the first experimental campaigns are also presented.

1. Introduction

From the design phase of the ROSPHERE γ-ray spectrometer, special attention was paid in order to meet the requirements of experiments devoted to measurements of excited nuclear state lifetimes over a wide range of values. Nuclear lifetimes are among the observables that are most sensitive to the underlying structure of the states, their knowledge providing information on the wave-functions (through the reduced matrix elements) of the states involved in the transition. During the past several years, the experimental programme at the Bucharest 9 MV Tandem accelerator was focused on such measurements. The recent series of experiments dedicated to this subject covered a wide range of nuclear lifetimes from tens of femtoseconds (using Doppler Shift Attenuation Method [1]), through the picosecond range (using the RDDS method [2,3]) up to the nanosecond range (using the new in-beam fast-timing method [4]). The physics cases covered a wide range of topics, including:

- the role of the negative-parity neutron intruder orbitals in the structure of low-spin states configurations for nuclei near the "island of inversion" [5,6];
- the study of the nuclear structure near shell and/or subshell closures [7–14], including the occurrence of intruder states [15];
- the interplay between collective and single-particle degrees of freedom [12,13];
- the study of neutron-rich nuclei using low energy transfer/incomplete fusion reactions induced by ^{7}Li beams [13,16–18].

Most of these experiments were performed with an evolving setup, with an increasing number of detectors (as many as available at the time) and geometries. Following the acquisition of more detectors, the design of an array was pursued, that would

* Corresponding author.
E-mail address: cmihai@tandem.nipne.ro (C. Mihai).

http://dx.doi.org/10.1016/j.nima.2016.08.052
0168-9002/

provide a stable geometrical setup and the possibility to accommodate various detector types. The result was the ROSPHERE array, dedicated to γ-ray spectroscopy, and especially suited to lifetime measurements using the RDDS and in-beam fast-timing methods. The ROSPHERE spectrometer is installed at the Bucharest 9 MV Tandem accelerator that was recently completely reconditioned [19–21] and is being operated by the Nuclear Physics Department (DFN) of the "Horia Hulubei" National Institute of Physics and Nuclear Engineering (IFIN-HH). The aim of this article is to describe the ROSPHERE array, its geometry, detectors and parameters, and to present results of several commissioning experiments dedicated to lifetime measurements of excited states. The RDDS method was used in ^{119}Te, the in-beam fast-timing method in ^{92}Zr, while both methods were used to measure the lifetime of the 11^- state in ^{150}Gd. Results from several fast-timing experiments using the ROSPHERE array were already published [9,10,14,22].

2. The ROSPHERE array

The ROSPHERE array can accommodate up to 25 detectors, the most used configuration being a "mixed" one, which combines Compton suppressed large volume HPGe detectors and fast $LaBr_3$(Ce) scintillators, optionally coupled with the plunger device, thus allowing in-beam fast-timing and RDDS measurements. Optionally ROSPHERE can be operated as a full HPGe array, for cases that require a high resolution and high efficiency detection system. ROSPHERE is equipped with two types of coaxial p-type HPGe detectors, commercially available from either ORTEC (type *a*) or CANBERRA (type *b*) with 50–60% relative efficiency, that requires two types of BGO shields and mounting flanges. In addition, planar low-energy photon (LEP) detectors can be mounted, providing high resolution detection capabilities for low energy photons. A pool of $LaBr_3$(Ce) scintillator crystals of various shapes and sizes is available and readout is provided via several types of photomultipliers.

The experimental activity with the ROSPHERE array is supported by two HPGe detector annealing stations, an electronics workshop and a state of the art target laboratory [23].

2.1. Geometry of the array

The ROSPHERE array was designed starting from a spherical configuration, taking into account the following requirements:

- compatibility with the plunger device;
- sensitivity for the Doppler effect, required by RDDS experiments (detectors placed at relatively small polar angles with respect to the beam axis);
- the possibility to obtain γ-ray multipolarity information (combination of detectors placed at angles with good sensitivity for directional correlation orientation (DCO) measurements);
- the possibility to mount large volume coaxial HPGe or LEP detectors (with their BGO shields) or $LaBr_3$(Ce) scintillator detectors in any position.

Using these conditions as the starting point, ROSPHERE was designed to have a spherical geometry, divided into five rings, each with five available positions for detectors. The 5 rings are placed at 37°, 70°, 90°, 110° and 143° with respect to the beam axis. This configuration is particularly suited to the measurement of DCO ratios of coincident transitions, thereby allowing γ-ray multipolarity determinations.

In order to maintain the spherical symmetry, the frame is an irregular polyhedron having as symmetry axes the beamline and the direction perpendicular to it, and consists of 27 flanges: 2 regular pentagons (along the beam axis), 10 irregular pentagons (the rings at 70° and 110°) and 15 irregular hexagons. In Fig. 1a, the geometry of the array is presented, with the five rings being distinguished by different colours. In order to provide access to the target chamber, the frame was designed to open into two asymmetric hemispheres (10 positions on the fixed backward hemisphere and 15 positions on the movable forward hemisphere) by sliding along the beam axis. CAD views of the array's support system, together with the rails that allow the forward hemisphere to slide are presented in Fig. 1b. In Fig. 2, the array is shown open, in its usual mixed configuration with the HPGe and $LaBr_3$(Ce) detectors mounted on the frame and the plunger device at the centre of the spectrometer.

The design of each flange allows the mounting of either type of BGO shield in a fixed position, while the corresponding HPGe detectors slide in place along three positioning rods. The target-to-detector distance varies for each type of HPGe detector depending on the ring. The $LaBr_3$(Ce) scintillators can be mounted at variable target to detector distance (minimum 150 mm). Table 1 summarises the target-to-detector distance for each ring and HPGe detector type.

2.2. The HPGe detectors

As mentioned above, the ROSPHERE HPGe detectors are commercially available p-type coaxial detectors, produced either by ORTEC (type *a*) or CANBERRA (type *b*). The detectors have a relative efficiency of minimum 50% (typical values 50–59%) and a typical resolution (FWHM) of 1.9 keV at 1.33 MeV.

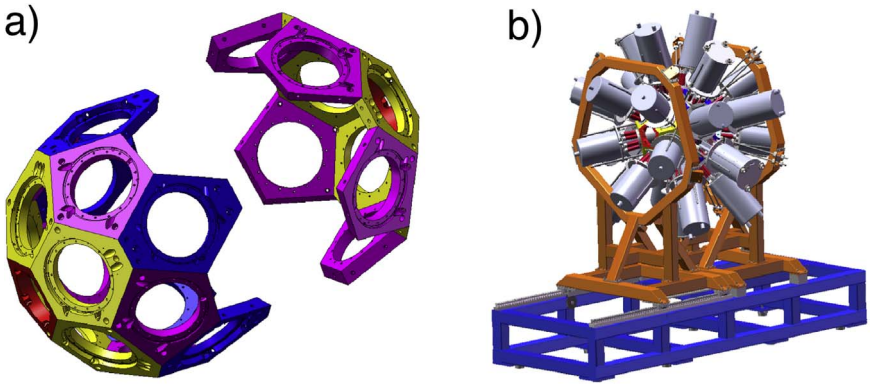

Fig. 1. (a) CAD view of the Geometry of the ROSPHERE array with the five rings distinguished by different colours, in yellow the 37° and 143° rings, in magenta the 70° and 110° rings and in blue the 90° ring, (b) CAD view of the frame, support system and HPGe detectors. (For interpretation of the references to color in this figure caption, the reader is referred to the web version of this paper.)

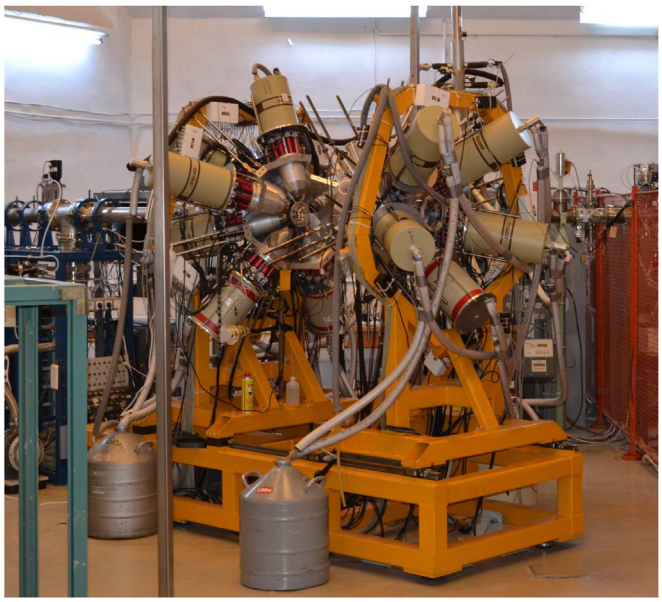

Fig. 2. View of the ROSPHERE array in the configuration used for the ^{119}Te experiment. The array is shown in the open position, with the endcap of the plunger device visible in the centre.

Table 1
Detector endcap to target distances for each type of HPGe detector and each ring.

Ring no.	No. of detectors	θ(degrees)	ϕ (degrees)	Distance type *a* (mm)	Distance type *b* (mm)
1 / 5	5 / 5	37 / 143	0, 72, 144, 216 and 288	179	210
2 / 4	5 / 5	70 / 110	36, 108, 180, 252 and 324	186	217
3	5	90	0, 72, 144, 216 and 288	176	208

The BGO shields were custom designed and manufactured by Scionix Holland BV. They consist of 8 optically separated trapezoid shaped BGO crystals with "nose" pieces, readout by 8 R6094 (type *a*) or 8 R3998 (type *b*) Hamamatsu PMTs. The BGO crystals have a thickness of maximum 29 mm and minimum 22 mm and a length of 178.6 mm (type *a*) and 146.6 mm (type *b*). A conical shaped Tungsten collimator is mounted at the front of the BGO crystals, shielding them from γ-rays emitted from the target position. Typical energy resolution is 18% at 661 keV. Fig. 3 shows CAD drawings of each type of HPGe detector and the corresponding BGO shield.

Optionally, up to four planar HPGe detectors can be mounted on the ROSPHERE frame, with a type *a* BGO shield, providing high resolution capabilities for low energy photons (FWHM 0.6 keV at 122 keV and 0.4 keV at 5.9 keV). The HPGe crystals are 36 mm in diameter and 10 mm thick, with a 0.3 μm Ge passive layer. The detectors are provided with a 0.25-mm thick Beryllium window.

The cooling and periodic refilling with LN_2 of up to 25 HPGe detectors is performed through a vacuum insulated manifold and transport pipe and an Auto-Fill control system, based on PLC industrial technology and built by the engineers of the IReS Strasbourg nuclear physics group for the CLARA array [24].

2.3. The $LaBr_3$(Ce) fast-timing detectors

As presented in Ref. [4], a fast-timing method suitable for *in-beam* γ-ray spectroscopy measurements was developed in our group, based on the use of the new $LaBr_3$(Ce) scintillators. These highly efficient scintillators have excellent properties concerning time resolution (100–300 ps depending on the crystal size) and energy resolution (typically 2–3% at 662 keV) due to the high light output per keV (more than 63 photons per keV) and fast decay time (~16 ns). A large pool of $LaBr_3$(Ce) crystals of various shapes and sizes is available for experiments with ROSPHERE, as summarised in Table 2.

The large light yield of the $LaBr_3$(Ce) crystal causes space charge effects in the PMT, leading to amplitude/energy non-linearity. To minimise these effects, $LaBr_3$(Ce) scintillators are usually read-out with special photomultiplier tubes with eight stages, such as the Photonis XP20d0 or the Hamamatsu R9779. The PMT's last dynode signal is used for the energy information, while the rapidly saturating anode signal is used for timing. Additionally, the PMTs are not operated at nominal voltage, but rather the optimum voltage that provides a linear energy response while preserving the timing properties is determined for each crystal/PMT pair.

2.4. Electronics and data acquisition

The electronics and data acquisition system of ROSPHERE is a reliable and stable system, consisting of standard NIM and CAMAC modules. The electronics block diagram, presented in Fig. 4 has two distinct components: a standard slow coincidence part to select the coincidence of at least n HPGe detectors (usually $n=2$ or 3) and a delayed coincidence part selecting the triple HPGe-$LaBr_3$(Ce)-$LaBr_3$(Ce) coincidences used for the fast-timing measurements. The delayed coincidence part is a slightly updated version of the block diagram discussed in detail in Ref. [4], the most important differences being:

- the use of a Timing Filter Amplifier (ORTEC quad TFA 863) with no integration or differentiation for the PMT's anode output, thus avoiding the low-energy cut that appears when using a Constant Fraction Discriminator (CFD) directly on the anode current output. The use of the TFA has little impact on the timing resolution, the results presented in Table 2 being similar to those reported earlier [4,27];
- the CFDs are used in the "blocking" mode (blocking window ≃800 ns) in order to clean the $LaBr_3$(Ce) time spectra of unwanted CFD multiple firing events.

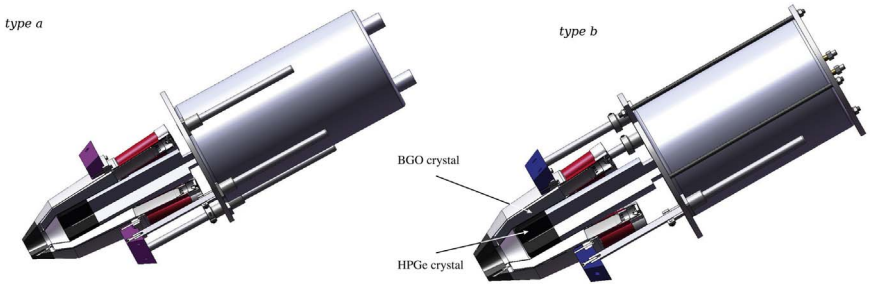

Fig. 3. CAD view of the ROSPHERE HPGe detectors with BGO shields and mounting system.

Table 2
Available $LaBr_3$(Ce) scintillator detectors. The dimensions of the crystals are given as height (H), diameter at the base (D) and diameter at the top (d).

Type No	Shape	No. of detectors	Dimensions $H \times D \times d$ (inch)	PMT	Timing resolution[a] (ps)
1	Cylindrical	3	$1.5 \times 1.5 \times 1.5$	Photonis XP20d0	182(2)
2	Cylindrical	7	$2 \times 2 \times 2$	Photonis XP5050	339(1)[b]
3	Conical	2	$1.5 \times 1.5 \times 1$	Photonis XP20d0	158(2)
4	Conical	3	$1.5 \times 1.5 \times 1$	Hamamatsu R9779	160[c]
5	Cylindrical	4	$2 \times 1.5 \times 1.5$	Hamamatsu R9779	191(2)[b]

[a] Defined as FWHM/$\sqrt{2}$ for the 1173–1332 keV coincident γ-rays from a ^{60}Co source, detected with a pair of identical detectors.
[b] Average values, see Fig. 5.
[c] From Ref. [27].

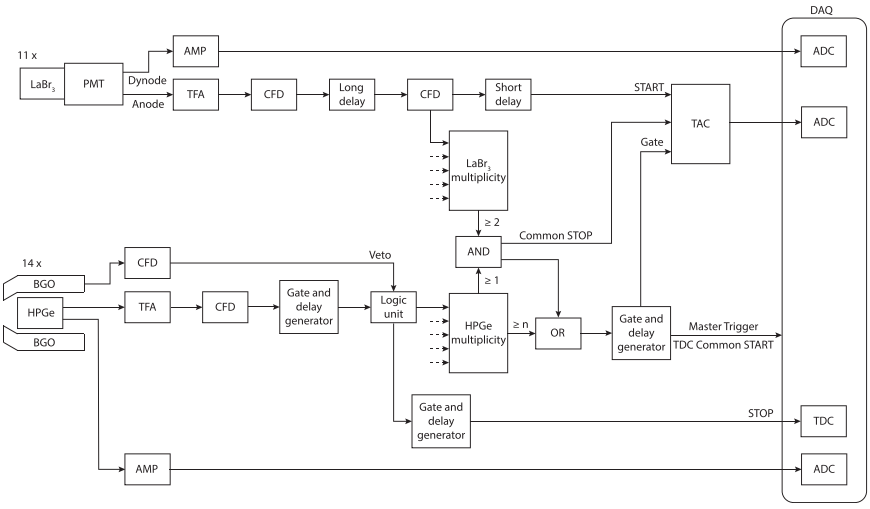

Fig. 4. Block diagram of the ROSPHERE electronics and data acquisition system.

As mentioned also in Ref. [4], the delays used in the delayed coincidence scheme are achieved only with cables of appropriate length, thus avoiding any additional jitter. The use of long delay cables (≃400 ns) distorts the shape of the timing signal, making necessary the use of a second discriminator after the long delay.

The master trigger signal is generated through an OR condition by either the slow coincidence scheme (corresponding to n HPGe detectors firing) or by the delayed coincidence scheme (corresponding to the HPGe-$LaBr_3$(Ce)-$LaBr_3$(Ce) detector combination). The master trigger serves as a common START for the HPGe Time-to-Digital converter. The two individual triggers are sufficiently spaced in time with respect to the HPGe STOP signal to allow an easy offline selection of the desired trigger combination. This master trigger construction is important because it allows simultaneous fast-timing measurements and measurements requiring HPGe coincidences (e.g. RDDS experiments).

The analogue FERA-bus fast CAMAC DAQ system was preferred for its proven stability and flexibility, and also availability of hardware and software solutions. The system is fully compatible with the GASPware data analysis programs [25]. The hardware consists of a CMC203 Fera Driver/Memory/Histogrammer, that provides rapid readout and event control over the FERA bus with a 1Mword buffer between the FERA data input and CAMAC data output, nine AD413A 4-channel, 13-bit Ortec Analogue-to-Digital Converters (ADC) used for the readout of HPGe energy information and $LaBr_3$(Ce) energy and timing (TAC) information and two 4418 T Silena TDC's used for the HPGe timing information. The data in event form are transferred through a Jorway 73A SCSI crate controller and stored on a local computer. The DAQ system is able to handle up to 2500 events/s without significant dead-time. Above this limit, the dead-time becomes significant rising to ≃50% at 5000 events/s.

2.5. The plunger device

In order to perform RDDS experiments with the ROSPHERE array, a plunger device was built, similar to the widely used Cologne coincidence plunger described in Ref. [26]. The RDDS method relies on the comparison of the lifetime of the level with the flight time of the recoil nucleus between the target and a stopper. The plunger device is used to achieve the required distance separations in the micrometre range. It consists of three systems:

- a mounting system housed in a spherical chamber at the centre of the array that allows the parallel mounting of the target and stopper with micrometre precision;
- a driving and control system consisting of an off-axis NEXACT N-381 piezoelectric actuator with a 25-mm travel range and 0.02-μm resolution, a stack of piezo-ceramics ("piezo-crystal") for short range corrections and an inductive micrometre probe to measure the travel distance with a 0.1-μm precision;
- a system of concentric tubes and sliding bearings that transfer the movement of the motor to the target frame. This is the most sensitive part of the plunger, as it has to transfer the off-axis linear motion of the actuator to the target frame while preserving the precision.

The target to stopper distance is kept constant by a feed-back system that uses the capacitance method to measure the distance and the piezo-crystal to correct beam induced drifts from the set

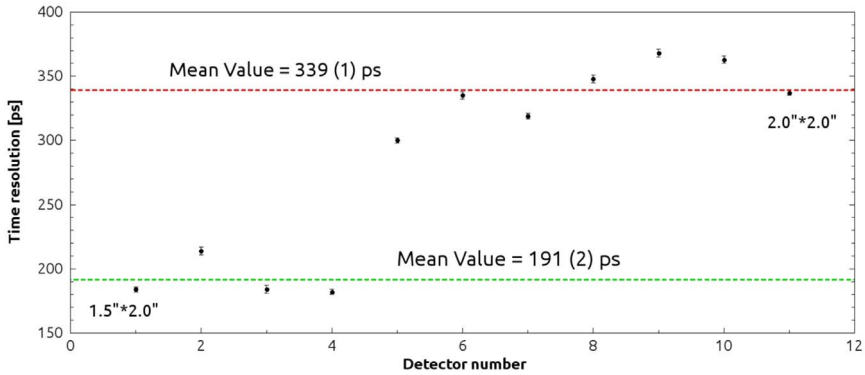

Fig. 5. Individual time resolution for the 11 $LaBr_3$(Ce) scintillator detectors used in the mixed configuration, measured as FWHM/$\sqrt{2}$ pairwise for identical detectors for the 1173–1332 keV coincident γ-rays from a ^{60}Co source.

Table 3
Performance parameters of the ROSPHERE array in the usual "mixed" configuration, measured with a ^{60}Co calibration source.

Sub-array	No. of detectors	Absolute efficiency @1332 keV	Peak/ total	Timing FWHM
HPGe	14	1.10(3)%	42%	≃15 ns
$LaBr_3$(Ce)	11	1.75(5) %	22%	347(10)[a] ps

[a] Overall FWHM of the time spectra for the 1173–1332 keV coincident γ-rays from a ^{60}Co source.

distance. The capacitance versus distance curve is measured before the experiment, using the inductive probe and the piezoelectric actuator's own travel measuring optical system.

2.6. Performance parameters in the mixed configuration

The ROSPHERE mixed configuration emerged as an optimum solution for running in-beam fast-timing and/or plunger experiments, while retaining sensitivity to DCO ratios. The usual mixed configuration comprises 14 HPGe detectors arranged in three rings (5 at 37°, 5 at 143° and 4 at 90°) and 11 $LaBr_3$(Ce) scintillators (seven crystals of type 2 and four crystals of type 5, see Table 2) arranged also in three rings (5 at 70°, 5 at 110° and 1 at 90°). The choice of the $LaBr_3$(Ce) scintillators used was a compromise between efficiency and time resolution, in the end the significantly higher efficiency of the type 2 and type 5 crystals being favoured over the better time resolution of the other types. The individual time resolution of the 11 $LaBr_3$(Ce) used in the ROSPHERE mixed configuration is shown in Fig. 5. The values were calculated as FWHM/ $\sqrt{2}$ for identical crystals, for the 1173–1332 keV coincidence from a ^{60}Co source. The overall FWHM of the time spectra for the $LaBr_3$(Ce) sub-array obtained for the 1173–1332 keV cascade was found to be 347(10) ps. The position of the HPGe detectors was chosen to be most sensitive in RDDS experiments, while the fast scintillators were placed in the remaining positions. Table 3 summarises the main parameters of the ROSPHERE spectrometer in the mixed configuration. The total efficiency of the array at 1.33 MeV is close to 3%, well balanced between the HPGe sub-array (1.10%) and $LaBr_3$(Ce) sub-array (1.75%).

3. Selected results from experimental campaigns

The first experiments with the ROSPHERE array, while having specific physics objectives, were also helpful in fine tuning the spectrometer by revealing potential problems and testing the sensitivity of the array in different configurations. Here we present lifetime results from several early ROSPHERE experiments, using the RDDS and in-beam fast-timing methods. The ROSPHERE array and the plunger device were used to measure lifetimes of excited states in ^{119}Te through the RDDS method, while the fast-timing method was used to measure lifetimes in the yrast band of ^{92}Zr. The mixed configuration also allows, in certain cases, a simultaneous and independent measurement of a lifetime by both RDDS and fast-timing methods. Such a combined RDDS and fast-timing measurement was performed in the case of the $J^\pi = 11^-$ state at 3366 keV in ^{150}Gd.

3.1. RDDS lifetime measurements in ^{119}Te

Excited states in ^{119}Te were populated in the ^{110}Pd(^{13}C, 4 n) reaction at a beam energy of 50 MeV. A 2-pnA ^{13}C beam impinged on a 0.7-mg/cm^2 99% enrichment self supported ^{110}Pd target mounted in the plunger device in front of a 4 mg/cm^2 gold stopper. Both foils were stretched on specially designed cones and were aligned inside the plunger device mounted in the centre of the ROSPHERE array. The experimental setup consisted of 14 HPGe detectors and 11 $LaBr_3$(Ce) scintillation detectors. For this experiment, the detector configuration was slightly different from the "mixed" configuration described in the previous section, 4 HPGe detectors being mounted in the 110° ring instead of the 90° ring. The fast scintillators occupied the remaining positions, the 70° and 90° rings accommodating 5 detectors each while the eleventh detector was mounted in the 110° ring. Data were recorded in event mode at 12 target-stopper distances ranging from the electrical contact point up to 60 μm. The data acquisition system was triggered by two HPGe detectors firing in coincidence or by the three fold HPGe-$LaBr_3$(Ce)-$LaBr_3$(Ce) coincidence.

The Differential Decay Curve Method (DDCM) [2,3] was used to extract the lifetimes from the experimentally determined intensities. The mean lifetime of the state of interest i is obtained by gating on the shifted component of a direct feeding transition and measuring the intensities of the shifted and unshifted peaks. The lifetime is then obtained using the formula:

$$\tau_i(d) = \frac{I_{uA}^{sB}(d)}{v\frac{d}{dt}I_{sA}^{sB}(d)}, \quad (1)$$

where v is the average velocity of the recoiling residual nucleus, A denotes the depopulating transition, B the directly feeding (and also gating) transition, $I_{uA}{}^{sB}$ and $I_{sA}{}^{sB}$ are the normalised intensities of the unshifted (u) and shifted (s) components of A detected in coincidence with the shifted component of B at a target-stopper distance d. Eq. (1) can be re-written as:

$$I_{uA}^{sB}(d) = v\tau_i \frac{d}{dt} I_{sA}^{sB}(d). \quad (2)$$

In practice, the differential term on the right-hand side of Eq. (2) is evaluated by fitting the shifted intensity $I_{sA}^{sB}(d)$ piecewise with continuous differentiable second order polynomials. The derivative of the resulting fit function is used to fit the unshifted intensity $I_{uA}^{sB}(d)$, up to a constant factor $v\tau$. Thus, the lifetime is obtained by the simultaneous fitting of both $I_{sA}^{sB}(d)$ and $I_{uA}^{sB}(d)$. The statistics of the data and the effective lifetime of the feeding level defines the so-called "region of sensitivity" around the maximum of the derivative term. In the DDCM analysis, one obtains an independent τ value for each distance within the sensitivity region with deviations from a constant value indicating systematic errors. The DDCM analysis is not affected by the deorientation effect [28] or by side feeding, and does not require an absolute distance calibration, only the relative target-stopper distances being used in the analysis.

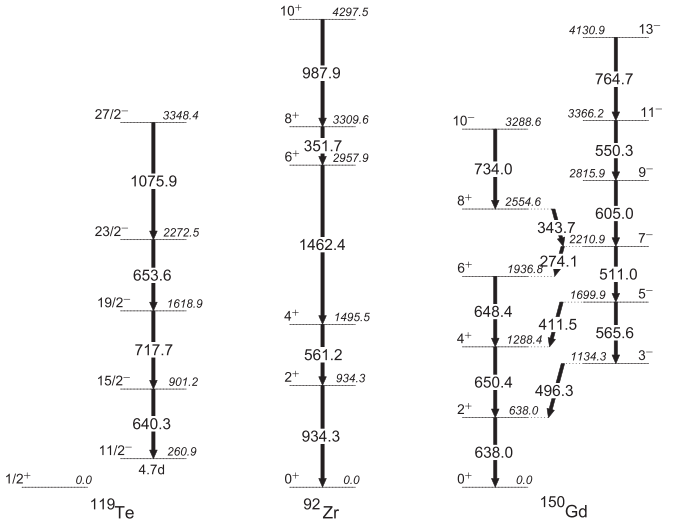

Fig. 6. Partial level schemes of ^{119}Te [29], ^{92}Zr [30] and ^{150}Gd [33], relevant for the experiments described in Section 3. The γ-ray transitions are labelled by their energy in keV.

For the DDCM analysis of this experiment, only the detectors placed in the rings at 37° (denoted "fw") and 143° ("bw") were used. The data were sorted into three energy-energy coincidence matrices for each distance, one asymmetric matrix having on one axis the detectors from the 37° ring and on the other axis the detectors from the 143° ring (denoted "fw-bw" matrix) and two symmetric matrices corresponding to the 37° ring ("fw-fw") and the 143° ring ("bw-bw") respectively.

In Fig. 6 a partial level scheme of ^{119}Te [29] is presented, showing the levels relevant for the DDCM analysis, belonging to the strongly populated negative-parity yrast band build on the $11/2^-$ isomer. Except for some isomeric states, no lifetime information for excited states was known for this nucleus [29] prior to the present measurement. In this experiment, lifetimes for the first three states in the band built on the $11/2^-$ isomer were determined. Fig. 7 shows the 640-keV transition de-exciting the $15/2^-$ state in ^{119}Te detected in the "bw" ring (left side panels) and in the "fw" ring (right side panels) at several target-stopper distances,

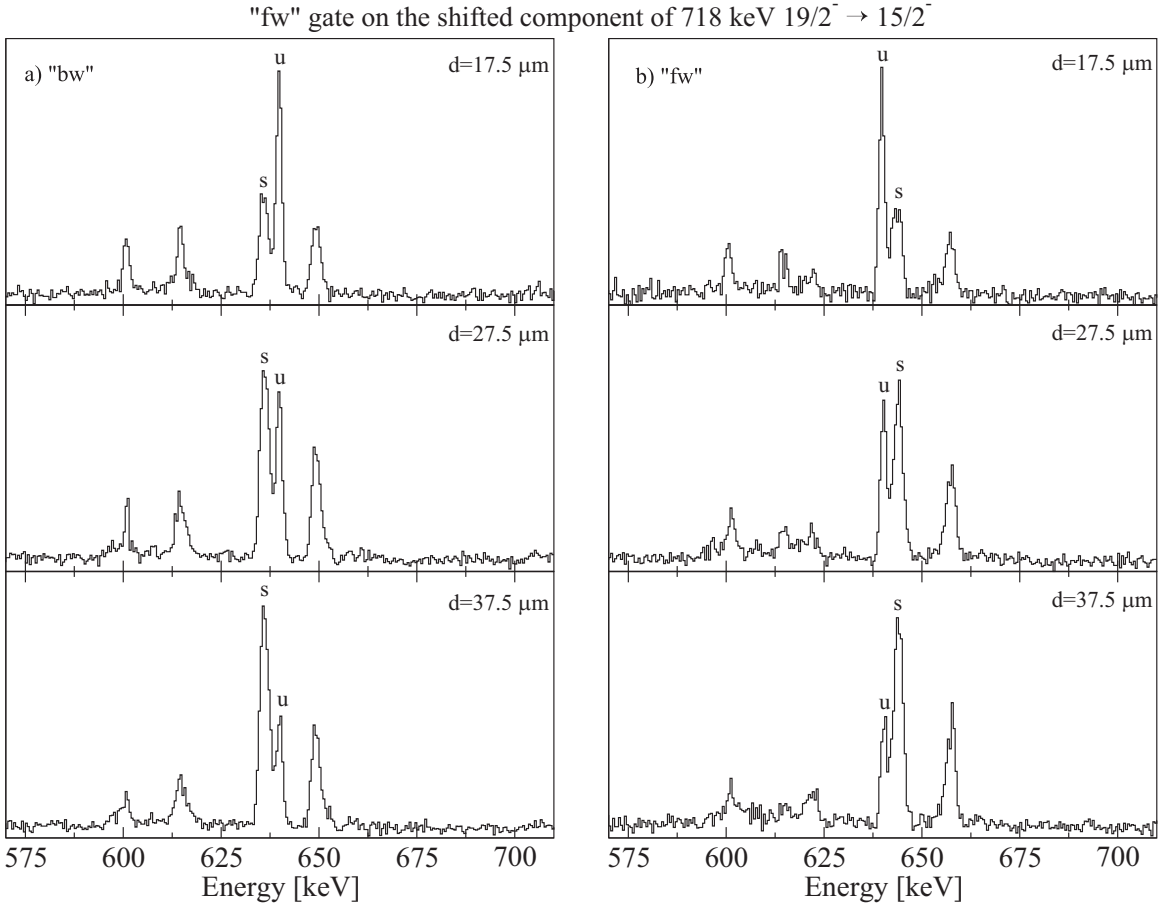

Fig. 7. Gated spectra of the 640-keV transition used to determine the lifetime of the $15/2^-$ state in ^{119}Te at various target-stopper distances, detected in (a) the 143° "bw" ring, (b) the 37° "fw" ring. The gate was set on the shifted component of the 718-keV transition.

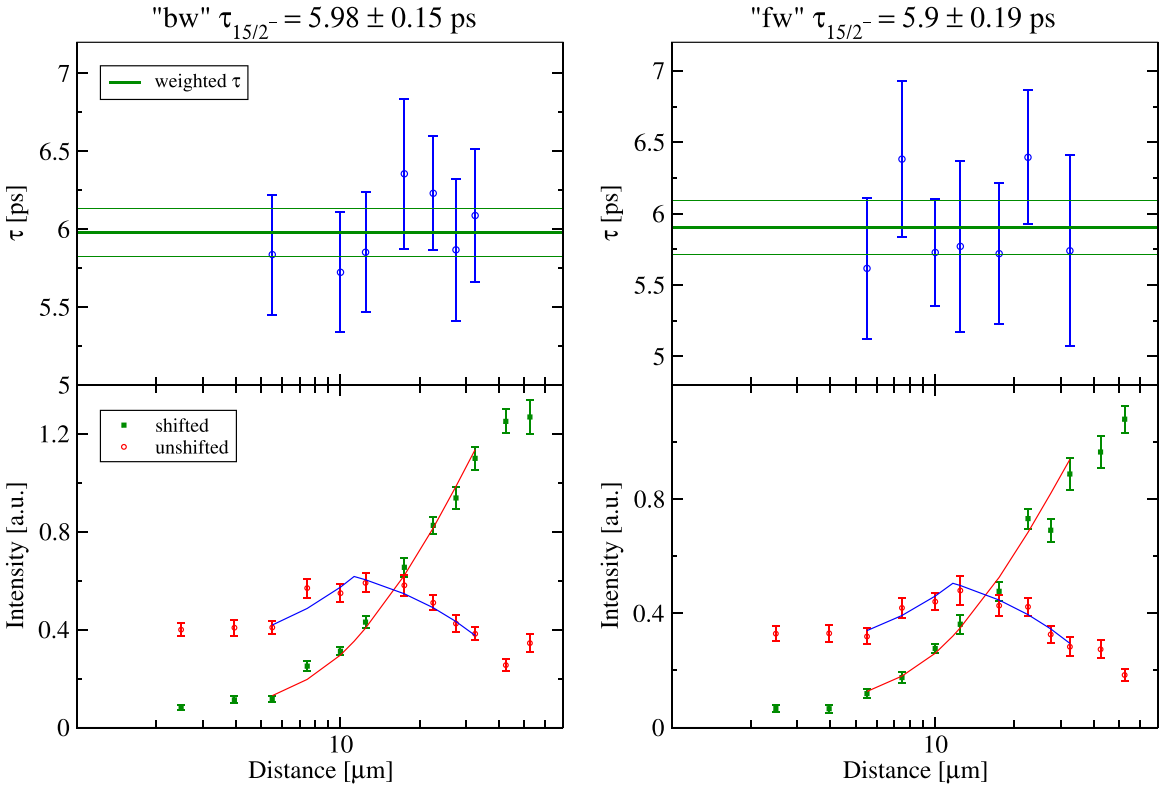

Fig. 8. DDCM analysis for the $15/2^-$ state for the "bw" ring (left panels) and "fw" ring (right panels). In the bottom panels, the symbols represent the experimentally measured intensities of the shifted component $I_{sA}^{sB}(d)$ (squares) and the unshifted component $I_{uA}^{sB}(d)$) (circles) while the curves represent the fits to each term of Eq. (2). The top panels show the τ values for each distance and the resulting mean lifetime. Only the points inside the "region of sensitivity" are included in the analysis.

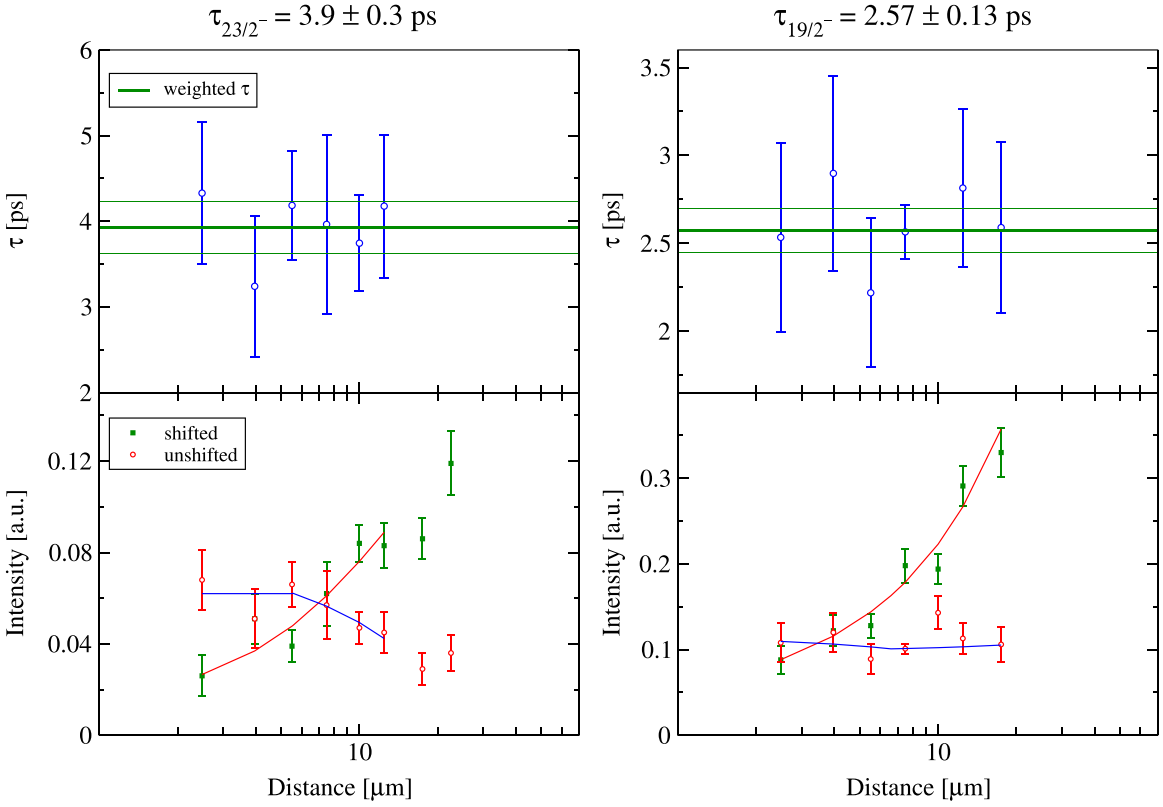

Fig. 9. As for Fig. 8 but for the $23/2^-$ state (left side panels) and $19/2^-$ state (right side panels) in ^{119}Te.

in coincidence with the shifted component of the 718-keV transition, detected in the "fw" ring. In the "bw" ring the shifted component of the 718-keV transition is overlapping with the 712-keV transition depopulating the 11^- state at 4086 keV in ^{120}Te, so could not be used in the analysis. The mean recoil velocity was measured to be $v/c = 0.75\%$ from the Doppler shift presented by several transitions.

Fig. 8 shows the DDCM analysis for the 640-keV transition and the corresponding mean lifetime of the $15/2^-$ state, performed for both "fw" and "bw" spectra (sample spectra presented in Fig. 7), directly gated by the shifted component of 718-keV transition detected in the "fw" ring. The analysis of the two sets of points gives results in good agreement, with a larger uncertainty in the case of the "fw" spectra due to lower statistics. Fig. 9 shows the similar DDCM analysis for the $23/2^-$ (left side panels) and $19/2^-$ (right side panels) states. The mean lifetime of the $19/2^-$ state was extracted from the analysis of the 718-keV transition (both in "fw" and "bw" rings, the latter being represented in Fig. 9), detected in coincidence with the shifted component of the directly feeding 653-keV transition. The mean lifetime of the $23/2^-$ state was extracted from the analysis of the 653-keV transition, detected in coincidence with the shifted component of the directly feeding 1075-keV transition. Table 4 presents the adopted mean lifetimes and the corresponding reduced transition probabilities. The uncertainties of the adopted mean lifetimes include a contribution from the uncertainty in the recoil velocity, unaccounted for in Figs. 8, 9.

3.2. Fast-timing lifetime measurements in ^{92}Zr

The mean lifetime of the yrast 4^+ state in ^{92}Zr, populated in the β decay of ^{92}Y was previously measured with the $\beta-\gamma$ fast-timing method to be $\tau = 147(5)$ ps in Ref. [31]. The lifetime of the yrast $J^\pi = 8^+$ level was measured in a recoil distance experiment to be $\tau = 1.7(1)$ ns [30,32]. Both level lifetimes are in the range of the in-beam fast-timing method and thus can be used to test the sensitivity of the ROSPHERE array.

In this experiment, a 42-MeV, 2-pnA ^{13}C beam delivered by the Bucharest 9 MV Tandem accelerator bombarded a 7-mg/cm^2 87% enriched ^{82}Se target on a 5 mg/cm^2 gold backing, populating excited states in ^{92}Zr in the 3 n evaporation channel. The γ-rays emitted following the reaction were detected with the ROSPHERE array in a similar configuration to the "mixed" one with 5 HPGe detectors at 37°, 5 at 143°, 3 at 90° and one at 110°, while the remaining positions were filled by the 11 $LaBr_3$(Ce) scintillators. The data were written in list mode, the DAQ trigger being set to either two HPGe detectors firing in coincidence or by the three-fold HPGe-$LaBr_3$(Ce)-$LaBr_3$(Ce) coincidence. The energy and efficiency calibrations for both the HPGe and $LaBr_3$(Ce) detectors were obtained using ^{152}Eu and ^{60}Co standard sources. Due to the gain instability of the $LaBr_3$(Ce) photomultipliers caused by the count rate fluctuations, a run-by-run gain matching procedure was applied. The timing response of each detector was corrected offline for the time walk effect using prompt γ-rays from the reaction, but also source data, as described in Refs. [4,22]. The half-lives of interest are evaluated from the time difference between populating and depopulating γ-rays, detected in pairs of fast scintillators. After calibrations, gain-shift and time-walk corrections, the data were sorted in $E_{\gamma1} - E_{\gamma2} - \Delta T$ cubes, following the procedure described in Ref. [4]. In order to cleanly select the transitions of interest, gates were placed on the 934, 561, 1462, 352 and 988-keV yrast transitions (see the level scheme in Fig. 6) detected in the HPGe detectors. In the bottom panel of Fig. 10 the summed spectra from the above mentioned gates applied on a HPGe $E_\gamma - E_\gamma$ symmetrical matrix is shown, while in the upper panel the total projection of the $E_{\gamma1} - E_{\gamma2} - \Delta T$ $LaBr_3$(Ce) cube, obtained with the same gating conditions, is presented.

Table 4
Adopted lifetimes and $B(E2)$ values for the analysed transitions in ^{119}Te.

E_x (keV)	J^π	E_γ (keV)	τ (ps)	B ($E2$) (W.u.)
901.2	$15/2^-$	640	5.9(4)	37(2)
1619.0	$19/2^-$	718	2.6(3)	48(5)
2272.4	$23/2^-$	653	3.9(5)	51(6)

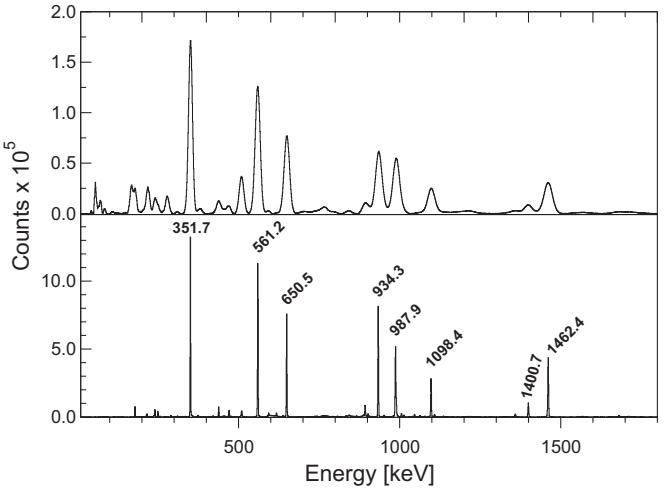

Fig. 10. γ-Ray energy spectra obtained by gating on the 934, 561, 1462, 352 and 988-keV yrast transitions in ^{92}Zr. Bottom: Summed gates in the HPGe-HPGe symmetric matrix; Top: Summed spectra from the $LaBr_3$(Ce) scintillators obtained with the same HPGe gates. The peaks are marked by their energy in keV.

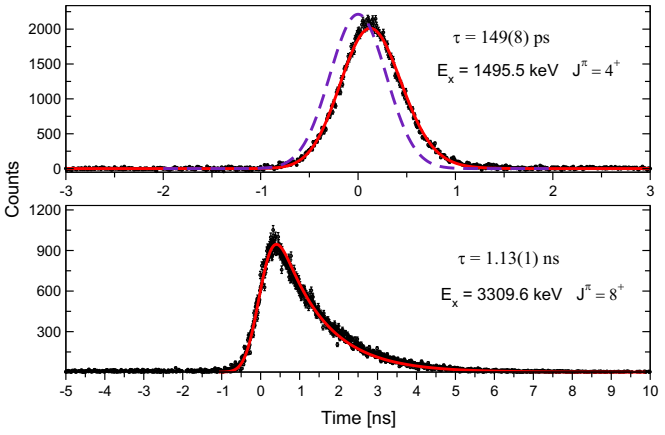

Fig. 11. Time distributions for the yrast 4^+ (upper panel) and 8^+ (bottom panel) states in ^{92}Zr, obtained by gating on the 462–561 keV and 988–352 keV, respectively as start–stop in the $E_{\gamma1} - E_{\gamma2} - \Delta T$ cubes. For both states, the half-life was obtained from the fit of the experimental data with the convoluted exponential decay function (red line), while the prompt response curve is shown in blue in the upper panel. (For interpretation of the references to color in this figure caption, the reader is referred to the web version of this paper.)

Fig. 11 shows the delayed coincidence time spectra for the 4^+ (upper panel) and 8^+ (bottom panel) yrast states, resulting from selecting the 1462–561 keV and 988–352 keV cascades, respectively as start-stop in the $E_{\gamma1} - E_{\gamma2} - \Delta T$ cubes. The experimental time spectra were fitted with exponential decay functions convoluted with a prompt response Gaussian function having an

experimentally measured width (for prompt transitions with similar energies). For the 1495.5 keV, 4^+ state, the fit resulted in a lifetime of $\tau = 149(8)$ ps, in good agreement with the 147(5) ps value from Ref. [31], obtained with the $\beta - \gamma$ fast-timing method using a thin plastic scintillator and a small BaF_2 crystal, resulting in a better time resolution. For the 3309.6 keV 8^+ state, the resulting lifetime of $\tau = 1.13(2)$ ns is in disagreement with the 1.7(1) ns value from Ref. [30]. We cannot comment on the recoil distance experiment [32], cited as the source of the value given in the evaluation [30], but we note that a *half-life* value of $T_{1/2} = 1.7(1)$ ns would result in a lifetime of $\tau = 1.18(7)$ ns, in agreement with our experimental value.

With careful calibrations and good experimental statistics, the in-beam fast-timing method has been demonstrated to work for lifetimes as low as 10 ps [22].

3.3. Combined RDDS and fast-timing lifetime measurement in ^{150}Gd

One of the advantages of the ROSPHERE array is the possibility to apply the RDDS and fast-timing methods in the same experiment, thus extending the range of accessible lifetimes from the picosecond range (using RDDS) to the nanosecond range (using fast-timing) and providing a consistency test for lifetimes accessible through both methods (in the range from tens to hundreds of picoseconds). Such an approach will also reduce the beamtime needed for an experiment by applying the fast-timing method (that uses the data from all target-stopper distances) to measure the lifetimes in the hundreds of picosecond to nanosecond range, while the RDDS method will be used to measure the shorter lifetimes. A plunger experiment on ^{150}Gd provided a test case for the combined RDDS and fast-timing measurement, the lifetime of the 11^- state at 3366 keV being predicted by the systematics to be in the overlapping region of both methods.

Excited states in ^{150}Gd were populated in the ^{140}Ce(^{13}C,3 n) reaction at a beam energy of 62 MeV. The target consisted of 0.5 mg/cm^2 of enriched ^{140}Ce, vacuum deposited on a 3-mg/cm^2 gold support, while the recoils were stopped in a 4-mg/cm^2 gold stopper, both foils being mounted in the plunger device at the centre of the ROSPHERE array. The average recoil velocity was measured to be $v/c = 0.7\%$. The γ-rays emitted in the reaction were detected in the ROSPHERE array in its "mixed" configuration. Data were recorded in event mode at 11 target-stopper distances ranging from the electrical contact point up to 500 μm. The data acquisition system was triggered by two HPGe detectors firing in coincidence or by the three-fold HPGe-$LaBr_3$(Ce)-$LaBr_3$(Ce) coincidence.

For the DDCM analysis of the lifetime of the 11^- state presented in the left panels of Fig. 12, the shifted and unshifted components of the 550-keV transition detected in coincidence with the shifted component of the directly feeding 765-keV transition were used to extract a mean lifetime value of 158(15) ps.

For the fast-timing analysis, a wide gate (including both shifted and unshifted components) was placed on the 565-keV transition in the HPGe spectra in order to select the 765–550 keV cascade in the $E_{\gamma 1} - E_{\gamma 2} - \Delta T$ cube and also to avoid any contamination from the 565-keV transition. The fast-timing analysis, presented in the left panel of Fig. 12, used the same 765–550 keV cascade to extract a mean lifetime value of 170(21) ps through the centroid shift method.

The values obtained by applying the two independent methods in the same experiment are in agreement considering the error bars, the small difference between the two values being attributed to poor statistics. A mean value of 162(12) ps was adopted for the lifetime of the 11^- state. This result confirms the validity of the combined RDDS and fast-timing approach.

4. Conclusions

The ROmanian array for SPectroscopy in HEavy ion REactions (ROSPHERE) was designed and installed at the Bucharest 9 MV Tandem accelerator as the main tool for γ-ray spectroscopy

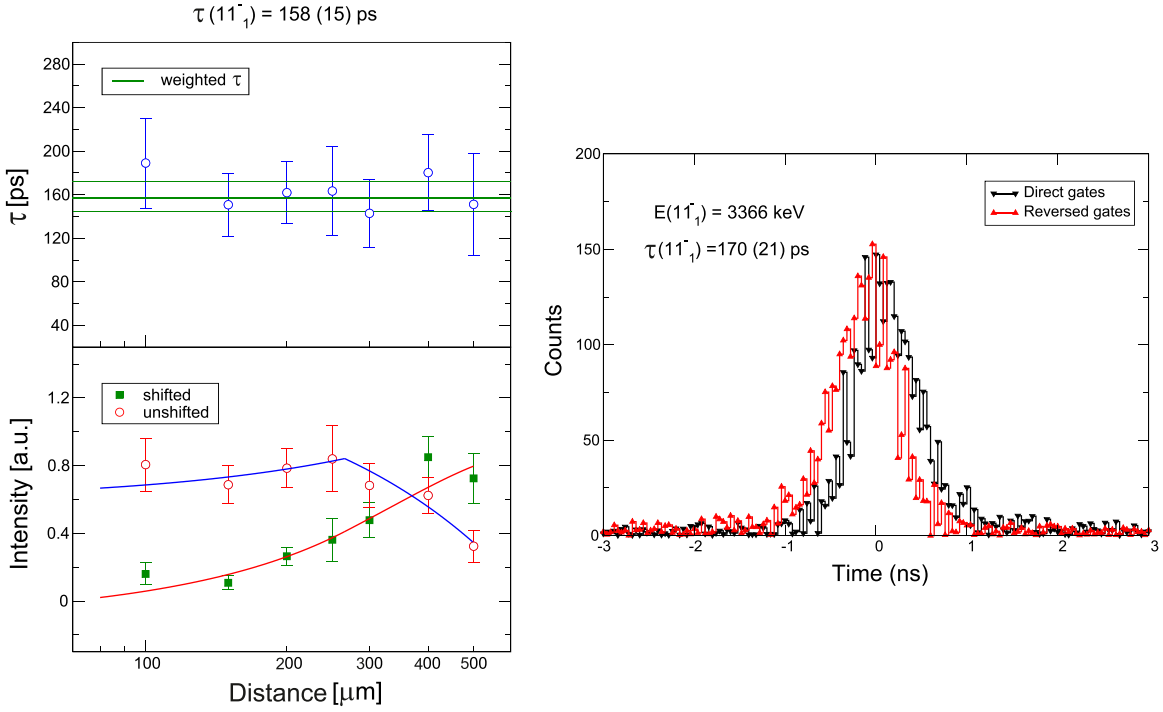

Fig. 12. Mean lifetime of the 11^- state at 3366 keV in ^{150}Gd. *Left*: DDCM analysis, similar with Fig. 8, *Right*: Time distribution for 765–550 keV start–stop combination (represented in black) in comparison with the reversed 550–765 keV combination (represented in red). The mean lifetime was obtained from the centroid shifts of the time distributions. (For interpretation of the references to color in this figure caption, the reader is referred to the web version of this paper.)

studies. In its usual mixed configuration, the array consists of 14 HPGe detectors with active Compton suppression and 11 fast $LaBr_3$(Ce) scintillators, which combined with a modern plunger device, allows lifetime measurements over a wide range. In order to illustrate the array's performance, results from several ROSPHERE experiments with the RDDS and in-beam fast-timing methods were presented.

The ROSPHERE array is an efficient and flexible tool for γ-ray spectroscopy, especially well suited for lifetime measurements over a range from picoseconds to nanoseconds. The array is available at the Bucharest FN TANDEM accelerator for γ-ray spectroscopy experiments proposed by the nuclear physics community.

Acknowledgements

We would like to thank the technical staff of the Bucharest Tandem accelerator for their contribution and support in the development and commissioning of the ROSPHERE array and for providing excellent beams for the experiments reported here. We would like to acknowledge the expertise and support from INCD COMOTI in the construction stage of the array, as well as the support of the companies (SCIONIX HOLLAND BV, ORTEC, CANBERRA, Saint Gobain Crystals) that provided part of the equipment. The loan of four $LaBr_3$(Ce) detectors from the UK-NUSTAR collaboration is acknowledged. We would like to thank the technical staff from the Institut für Kernphysik der Universität zu Köln for their support in the construction and commissioning of the plunger device. This work was supported by the Romanian Executive Unit for Financing Higher Education, Research, Development and Innovation (UEFISCDI) under contracts PNII-ID-PCE-2011-3-0367, PNII-CAPACITĂŢI/RO-CERN/F104 and PNII-RU-TE-2014-4-2003. A.M.B., Z.P., P.H.R. and O.J.R. acknowledge support from the Science and Technologies Facilities Council (STFC-UK). P. H.R. acknowledge support from the UK National Measurement Office (NMO).

References

[1] C. Mihai, A.A. Pasternak, D. Filipescu, M. Ivaşcu, D. Bucurescu, G. Cătа-Danil, I. Cătа-Danil, D. Deleanu, D. Ghiţă, T. Glodariu, Yu.N. Lobach, N. Mărginean, R. Mărginean, A. Negret, S. Pascu, T. Sava, L. Stroe, G. Suliman, N.V. Zamfir, Phys. Rev. C81 (2010) 034314.
[2] A. Dewald, S. Harissopulos, P. von Brentano, Z. Phys. A 334 (1989) 163.
[3] G. Böhm, A. Dewald, P. Petkov, P. von Brentano, Nucl. Instrum. Methods Phys. Res. A 339 (1993) 248.
[4] N. Mărginean, D.L. Balabanski, D. Bucurescu, S. Lalkovski, L. Atanasova, G. Cătа-Danil, I. Cătа-Danil, J.M. Daugas, D. Deleanu, P. Detistov, G. Deyanova, D. Filipescu, G. Georgiev, D. Ghiţă, K.A. Gladnishki, R. Lozeva, T. Glodariu, M. Ivaşcu, S. Kisyov, C. Mihai, R. Mărginean, A. Negret, S. Pascu, D. Radulov, T. Sava, L. Stroe, G. Suliman, N.V. Zamfir, Eur. Phys. J. A46 (2010) 329–336.
[5] P.J.R. Mason, T. Alharbi, P.H. Regan, N. Mărginean, Zs. Podolyak, E.C. Simpson, N. Alkhomashi, P.C. Bender, M. Bowry, M. Bostan, D. Bucurescu, A.M. Bruce, G. Cătа-Danil, I. Cătа-Danil, R. Chakrabarti, D. Deleanu, P. Detistov, M. N. Erduran, D. Filipescu, U. Garg, T. Glodariu, D. Ghiţă, S.S. Ghugre, A. Kusoglu, R. Mărginean, C. Mihai, M. Nakhostin, A. Negret, S. Pascu, C. Rodriguez Triguero, T. Sava, A.K. Sinha, L. Stroe, G. Suliman, N.V. Zamfir, Phys. Rev. C85 (2012) 064303.
[6] T. Alharbi, P.J.R. Mason, P.H. Regan, Zs. Podolyak, N. Mărginean, M. Nakhostin, M. Bowry, D. Bucurescu, G. Cătа-Danil, I. Cătа-Danil, D. Deleanu, D. Filipescu, T. Glodariu, D. Ghiţă, R. Mărginean, C. Mihai, A. Negret, S. Pascu, T. Sava, L. Stroe, G. Suliman, N.V. Zamfir, A.M. Bruce, C. Rodriguez Triguero, P.C. Bender, U. Garg, M.N. Erduran, A. Kusoglu, M. Bostan, P. Detistov, N. Alkhomashi, A. K. Sinha, R. Chakrabarti, S.S. Ghugre, Appl. Rad. Isot. 70 (2012) 1337.
[7] C. Kuppersbusch, S. Pascu, P. von Brentano, D. Bucurescu, Gh. Cătа-Danil, D. Deleanu, J. Endres, M. Elvers, D. Filipescu, C. Friessner, D.G. Ghiţă, T. Glodariu, C. Mihai, N.M. Mărginean, R. Mărginean, A. Negret, T. Sava, L. Stroe, V. Werner, N.V. Zamfir, K.-O. Zell, A. Zilges, Eur. Phys. J. A48 (2012) 1.
[8] T. Alharbi, P.H. Regan, P.J.R. Mason, N. Mărginean, Z. Podolyak, A.M. Bruce, E. C. Simpson, A. Algora, N. Alazemi, R. Britton, M.R. Bunce, D. Bucurescu, N. Cooper, D. Deleanu, D. Filipescu, W. Gelletly, D. Ghiţă, T. Glodariu, G. Ilie, S. Kisyov, J. Lintott, S. Lalkovski, S. Liddick, C. Mihai, K. Mulholland, R. Mărginean, A. Negret, M. Nakhostin, C.R. Niţă, O.J. Roberts, S. Rice, J.F. Smith, L. Stroe, T. Sava, C. Townsley, E. Wilson, V. Werner, M. Zhekova, N.V. Zamfir, Phys. Rev. C87 (2013) 014323.
[9] T. Alharbi, P.H. Regan, N. Mărginean, Zs. Podolyak, A. Bajoga, R. Britton, D. Bucurescu, D. Deleanu, D. Filipescu, D. Ghiţă, T. Glodariu, C. Mihai, K. Mulholland, R. Mărginean, A. Negret, C.R. Niţă, Z. Patel, O.J. Roberts, L. Stroe, T. Sava, C. Townsley, N.V. Zamfir, Nucl. Data Sheets 120 (2014) 59.
[10] T. Alharbi, P.H. Regan, N. Mărginean, Zs. Podolyk, O.J. Roberts, A.M. Bruce, N. Alkhomashi, R. Britton, D. Bucurescu, D. Deleanu, D. Filipescu, D. Ghţă, T. Glodariu, C. Mihai, K. Mulholland, R. Lică, R. Mărginean, M. Nakhostin, A. Negret, C.R. Niţă, L. Stroe, T. Sava, C. Townsley, N.V. Zamfir, Phys. Rev. C91 (2015) 027302.
[11] S. Kisyov, S. Lalkovski, N. Mărginean, D. Bucurescu, L. Atanasova, D. L. Balabanski, G. Cătа-Danil, I. Cătа-Danil, J.-M. Daugas, D. Deleanu, P. Detistov, D. Filipescu, G. Georgiev, D. Ghiţă, T. Glodariu, J. Jolie, D.S. Judson, R. Lozeva, R. Mărginean, C. Mihai, A. Negret, S. Pascu, D. Radulov, J.M. Regis, M. Rudigier, T. Sava, L. Stroe, G. Suliman, N.V. Zamfir, K.O. Zell, M. Zhekova, Phys. Rev. C84 (2011) 014324.
[12] C. Michelagnoli, C.A. Ur, E. Farnea, S. Lenzi, S. Lunardi, F. Recchia, N. Mărginean, D. Bucurescu, G. Cătа-Danil, D. Deleanu, D. Filipescu, D. Ghiţă, T. Glodariu, R. Mărginean, C. Mihai, A. Negret, S. Pascu, T. Sava, L. Stroe, G. Suliman, Acta Physica Pol. B42 (2011) 825.
[13] C.R. Niţă, D. Bucurescu, N. Mărginean, M. Avrigeanu, G. Bocchi, S. Bottoni, A. Bracco, A.M. Bruce, G. Cătа-Danil, G. Colo, D. Deleanu, D. Filipescu, D. G. Ghiţă, T. Glodariu, S. Leoni, C. Mihai, P.J.R. Mason, R. Mărginean, A. Negret, D. Pantelica, Z. Podolyak, P.H. Regan, T. Sava, L. Stroe, S. Toma, C.A. Ur, E. Wilson, Phys. Rev. C89 (2014) 064314.
[14] G. Bocchi, S. Leoni, S. Bottoni, G. Benzoni, A. Bracco, P.F. Bortignon, G. Colo, B. Belvito, C.R. Niţă, N. Mărginean, D. Filipescu, D. Ghiţă, T. Glodariu, R. Lică, R. Mărginean, C. Mihai, A. Negret, T. Sava, L. Stroe, S. Toma, D. Bucurescu, I. Georghe, R. Suvaila, D. Deleanu, C.A. Ur, S. Aydin, Phys. Rev. C89 (2014) 054302.
[15] C. Mihai, A.A. Pasternak, S. Pascu, D. Filipescu, M. Ivaşcu, D. Bucurescu, G. Cătа-Danil, I. Cătа-Danil, D. Deleanu, D.G. Ghiţă, T. Glodariu, N. Mărginean, R. Mărginean, A. Negret, T. Sava, L. Stroe, G. Suliman, N.V. Zamfir, Phys. Rev. C83 (2011) 54310.
[16] O.J. Roberts, A.M. Bruce, F. Browne, N. Mărginean, T. Alexander, T. Alharbi, D. Bucurescu, D. Deleanu, D. Delion, D. Filipescu, L. Fraile, I. Gheorghe, D. Ghiţă, T. Glodariu, D. Ivanova, S. Kisyov, R. Mărginean, P.J.R. Mason, C. Mihai, K. Mulholland, A. Negret, C. Niţă, B. Olaizola, S. Pascu, P.A. Soderstrom, P. H. Regan, T. Sava, L. Stroe, S. Toma, C. Townsley, Acta Physica Pol. B44 (2013) 403–406.
[17] D. Deleanu, D.L. Balabanski, Ts. Venkova, D. Bucurescu, N. Mărginean, E. Ganioglu, Gh. Cătа-Danil, L. Atanasova, I. Cătа-Danil, P. Detistov, D. Filipescu, D. Ghiţă, T. Glodariu, M. Ivaşcu, R. Mărginean, C. Mihai, A. Negret, S. Pascu, T. Sava, L. Stroe, G. Suliman, N.V. Zamfir, Phys. Rev. C87 (2013) 014329.
[18] P.J.R. Mason, Zs. Podolyak, N. Mărginean, P.H. Regan, P.D. Stevenson, V. Werner, T. Alexander, A. Algora, T. Alharbi, M. Bowry, R. Britton, A.M. Bruce, D. Bucurescu, M. Bunce, G. Cătа-Danil, I. Cătа-Danil, N. Cooper, D. Deleanu, D. Delion, D. Filipescu, W. Gelletly, D. Ghiţă, I. Gheorghe, T. Glodariu, G. Ilie, D. Ivanova, S. Kisyov, S. Lalkovski, R. Lică, S.N. Liddick, R. Mărginean, C. Mihai, K. Mulholland, C.R. Niţă, A. Negret, S. Pascu, S. Rice, O.J. Roberts, T. Sava, J. F. Smith, P.-A. Soderstrom, L. Stroe, G. Suliman, R. Suvaila, S. Toma, C. Townsley, E. Wilson, R.T. Wood, M. Zhekova, C. Zhou, Phys. Rev. C88 (2013) 044301.
[19] D.G. Ghiţă, D.V. Moşu, M. Dogaru, M.M. Gugiu, I.V. Popescu, I.C. Călinescu, Gh. Cătа-Danil, M. Enăchescu, N. Mărginean, A. Pantelica, D. Pantelica, A. Petre, T.B. Sava, C.A. Simion, C. Stan-Sion, M. Statescu, P. Ionescu, N.V. Zamfir, Application of accelerators in research and industry, AIP Conf. Proc. 1525 (2013), 208–213.
[20] D.V. Moşu, D.G. Ghiţă, S. Dobrescu, T. Sava, I.O. Mitu, I.C. Calinescu, G. Naghel, G. Dumitru, Gh. Cătа-Danil, Nucl. Instrum. Methods Phys. Res. A 693 (2012) 143–147.
[21] D.V. Moşu, D.G. Ghiţă, S. Dobrescu , T. Sava , B. Savu , G. Naghel , D. Moisa , I.C. Calinescu , G. Dumitru , I.O. Mitu, M. Petcu, Gh. Cătа-Danil, Nucl. Instrum. Methods Phys. Res. A 707 40–44.
[22] S. Pascu, D. Bucurescu, Gh. Cătа-Danil, V. Derya, M. Elvers, D. Filipescu, D. G. Ghiţă, T. Glodariu, A. Hennig, C. Mihai, N. Mărginean, R. Mărginean, A. Negret, L. Netterdon, S.G. Pickstone, T. Sava, M. Spieker, L. Stroe, N.V. Zamfir, A. Zilges, Phys. Rev. C. 91 (2015) 034321.
[23] N.M. Florea, L. Stroe, R. Mărginean, D.G. Ghiţă, D. Bucurescu, M. Badea, C. Costache, R. Lică, N. Mărginean, C. Mihai, D.V. Moşu, C.R. Niţă, S. Pascu, T. Sava, J. Radioanal. Nucl. Chem. 305 (2015) 707.
[24] A. Gadea, et al., Eur. Phys. J. A 20 (2004) 193.
[25] D. Bazzaco, N. Mărginean, private communication.
[26] A. Dewald, O. Möller, P. Petkov, Prog. Part. Nucl. Phys. 67 (2012) 786–839.
[27] O.J. Roberts, A.M. Bruce, P.H. Regan, Z. Podolyak, C.M. Townsley, J.F. Smith, K. F. Mulholland, A. Smith, Nucl. Instrum. Methods Phys. Res. A 748 (2014) 91–95.
[28] P. Petkov, Nucl. Instrum. Methods Phys. Res. A 349 (1994) 289.
[29] D.M. Symochko, E. Browne, J.K. Tuli, Nucl. Data Sheets 110 (2009) 2945.
[30] C.M. Baglin, Nucl. Data Sheets 113 (2012) 2187.
[31] H. Mach, E.K. Warburton, W. Krips, R.L. Gill, M. Moszynski, Phys. Rev. C. 42 (1990) 568.
[32] G. Korschinek, M. Fenzl, H. Hick, A.J. Kreiner, W. Kutschera, E. Nolte, H. Morinaga, Proceedings of the International Conference on Nuclear Structure, Tokyo, vol.1, p. 326 (1977).
[33] S.K. Basu, A.A. Sonzogni, Nucl. Data Sheets 114 (2013) 435.